AIP Journal of Applied Physics

Uniaxial magnetic anisotropy for thin Co films on glass studied by magnetooptic Kerr effect

T. Kuschel, T. Becker, D. Bruns, M. Suendorf, F. Bertram, P. Fumagalli, and J. Wollschläger

Citation: Journal of Applied Physics **109**, 093907 (2011); doi: 10.1063/1.3576135
View online: http://dx.doi.org/10.1063/1.3576135
View Table of Contents: http://scitation.aip.org/content/aip/journal/jap/109/9?ver=pdfcov
Published by the AIP Publishing

Uniaxial magnetic anisotropy for thin Co films on glass studied by magnetooptic Kerr effect

T. Kuschel,[1] T. Becker,[1] D. Bruns,[1] M. Suendorf,[1] F. Bertram,[2] P. Fumagalli,[3] and J. Wollschläger[1,a)]
[1]*Fachbereich Physik, Universität Osnabrück, Barbarastraße 7, D-49069 Osnabrück, Germany*
[2]*Hamburger Synchrotronstrahlungslabor am Deutschen Elektronen-Synchrotron, Notkestraße 85, D-22607 Hamburg, Germany*
[3]*Institut für Experimentalphysik, Freie Universität Berlin, Arnimallee 14, D-14195 Berlin, Germany*

(Received 21 December 2010; accepted 14 March 2011; published online 5 May 2011)

Thin Co films of different thickness deposited on glass are investigated by magnetooptic Kerr effect to study the uniaxial magnetic anisotropy of these films. The direction of the uniaxial magnetic anisotropy is determined from the azimuthal dependence of the magnetic remanence and differs with increasing thickness of the Co film investigated by x-ray reflectivity. Our experiments reveal that preparation conditions like temperature, deposition rate, or obliqueness of deposition cannot be the reason for this rotation effect of the uniaxial magnetic anisotropy. Also, strain in the substrate and possible textures in the film structure can be excluded as the origin of the magnetic behavior as studied by grazing incidence wide angle x-ray scattering. Thus, probably only the substrate shape in connection with the amorphous or polycrystalline film structure can explain the rotation of the uniaxial magnetic anisotropy. © *2011 American Institute of Physics*.
[doi:10.1063/1.3576135]

I. INTRODUCTION

The origin of a uniaxial magnetic anisotropy (UMA) in thin ferromagnetic films is often related to preparation conditions or substrate properties. For example, using molecular beam epitaxy (MBE) the angle of incidence of the molecular beam can influence the magnetic properties of the deposited film due to in-plane tetragonal distortion of the crystal structure as demonstrated for the case of epitaxial thin films of Fe on MgO.[1,2] Also, strained films or thin films deposited on vicinal substrates can exhibit a UMA, e.g., Fe films grown on vicinal Au(001) are examined.[3]

The magnetic anisotropy of unicrystalline Co films can be affected by temperature, processing, and underlayer.[4] For polycrystalline Co films on glass it is assumed that a UMA is caused by the shape or microstructure of the substrate or by an obliqueness of deposition as reported for Co films less than 200 nm thick.[5,6]

Here, we report on thin Co films of thicknesses between 8.5 and 90 nm which are deposited on glass substrates to investigate effects due to the UMA. The structural characterization of the films included x-ray reflectivity (XRR) and grazing incidence wide angle x-ray scattering (GIWAXS) as well as atomic force microscopy (AFM). The magnetic properties were determined by the magnetooptic Kerr effect (MOKE) at room temperature.

II. EXPERIMENT

All Co films were prepared by MBE in a high vacuum chamber at room temperature using electron beam evaporation. Ultra-thin Co films (film thickness <20 nm) were deposited by evaporation from a rod by heating the material with accelerated electrons (applied voltage 1 kV). The pressure in the preparation chamber was $p = 10^{-6}$ mbar (base pressure at $p = 10^{-7}$ mbar). The glass substrates (10×10 mm^2) were cut out of bigger glass plates to have similar substrates. Before each glass substrate was transferred into the preparation chamber, it had been cleaned in isopropanol using ultrasonic agitation. The Co deposition rate was 0.3 nm/min at an angle of about 8° with respect to normal incidence. The films were capped by amorphous Si to avoid oxidation after transfer to ambient conditions. Si was evaporated using an effusion cell.

Thicker Co films (film thickness ≥50 nm) were grown by deposition from commercial electron beam evaporator at a base pressure of $p = 10^{-9}$ mbar (Co deposition rate of 12 nm/min). These films were not capped by Si prior to transfer to ambient conditions, so that the Co surface was oxidized.

In order to fabricate films with well defined thicknesses we used a quartz crystal monitor for the ultra-thin films. This monitor was calibrated *a posteriori* by comparison with XRR results obtained for three Co films of different thickness.

The XRR measurements were performed by synchrotron radiation in $\vartheta - 2\vartheta$ scattering geometry at beamline W1 at DORIS III (DESY, Hamburg, Germany) with a photon energy of 10.5 keV ($\lambda = 1.18$ nm). Furthermore, XRR experiments were done at beamline BL9 at DELTA (Technische Universität Dortmund, Germany) with a photon energy of 15.5 keV ($\lambda = 0.80$ nm). In order to obtain the thickness of the Co films and the roughness of the interfaces, the XRR data had been analyzed using the recursive Parratt algorithm[7] and the in-house developed analysis tool *i*XRR.[8]

2D GIWAXS patterns were taken at DELTA using a 2D MAR345 image plate detector to probe the polycrystallinity of the Co films at grazing incidence of the x-ray beam which increases the sensitivity of the experiment to the Co film.

a)Electronic mail: joachim.wollschlaeger@uos.de.

The angle of incidence was $\vartheta = 0.5°$, which is above the critical angle ϑ_c at 15.5 eV of both Si ($\vartheta_c = 0.1°$) and Co ($\vartheta_c = 0.2°$). Thus, the penetration depth of the x-rays for our system is at least 1.5 μm for an angle of incidence of $\vartheta = 0.5°$, so the incident beam passes through all films and penetrates large parts of the substrate.

For the AFM measurements, the contact AFM Nanosurf easyScan 2 was used under ambient conditions (lateral resolution 40 nm, vertical resolution 0.5 nm).

The MOKE setup is built up in the longitudinal geometry, so that the magnetic field is aligned parallel to the surface of the sample and parallel to the plane of incidence of light. A He-Ne-Laser with the wavelength of $\lambda = 632.8$ nm and an angle of incidence of 45° is used. The incident light is s-polarized (perpendicular to the plane of incidence of light). The polarization of the reflected beam is modulated by a photo-elastic modulator (PEM) with a modulation frequency of $f = 50$ kHz. The rotation of the polarization of the reflected beam is proportional to the magnetization of the film. This Kerr rotation of the polarized signal is transformed into an intensity signal using a second polarizer behind the PEM, which is rotated by 45° with respect to the plane of incidence of light. The lock-in technique provides the Kerr rotation reading out the $2f$-signal.[9] The magnetization curves were measured for several in-plane directions of the sample by varying the magnetic field $\mu_0 H$ between -5 mT and $+5$ mT, which was recorded by a Hall probe, and by receiving the Kerr rotation signal.

III. RESULTS

A. XRR results

The x-ray reflectivity measurement of an exemplary Co film capped by amorphous silicon is presented in Fig. 1 (lower curve). The reflected x-ray intensity is plotted against the magnitude of the reciprocal scattering vector $q = 2k \sin \vartheta$. $k = 2\pi/\lambda$ denotes the wave number and ϑ the angle of incidence of the x-ray beam, respectively. The curve shows oscillations due to the interference of the beams reflected at both the surface of the Co film and the interface between the Co film and the glass substrate. Well resolved intensity oscillations show that the films have homogeneous thickness and very small interface roughness.

We calculate the reflectivity with a model of two layers shown in Fig. 1 (inset). The data can be well fitted assuming an 11.2 nm Co film with an interface roughness of 1.4 nm to the Si capping layer, a Si capping layer of 3.6 nm thickness with a roughness of 0.9 nm and a substrate roughness of 0.9 nm (upper solid curve in Fig. 1). Thus, a homogeneous Co film is grown on the glass substrate.

The AFM measurement of the Si capped 11.2 nm Co film shows a closed capping layer with few islands. In addition, we do not detect any pinholes of the capping layer. This indicates a dense growth of the capping material, which is an important condition to protect thin Co films from oxidation and degradation. The standard deviation of the height distribution of a 15×15 μm^2 area as obtained from the AFM experiments amounts to 1.0 nm which is in excellent agreement with the XRR results. Further, thinner Co films which are examined by XRR show similar characteristic parameters.

The XRR measurements of the thicker Co films, which are uncapped, can be modeled assuming an oxide layer above the Co film instead of a silicon cap. The thickness of the metallic Co films are 50 and 90 nm. The interface roughness is comparable to the ultra-thin Co films.

B. MOKE results

The magnetization curves show a typical ferromagnetic behavior as shown in Fig. 2 for the uncapped 50 nm Co film. The MOKE signal is proportional to the in-plane component of the magnetization vector parallel to the plane of incidence of light, since the out-of-plane component can be neglected because of the magnetic shape anisotropy. The MOKE signal is scaled to its saturation value and thus represents the relative magnetization M/M_s. The solid curve in Fig. 2 is

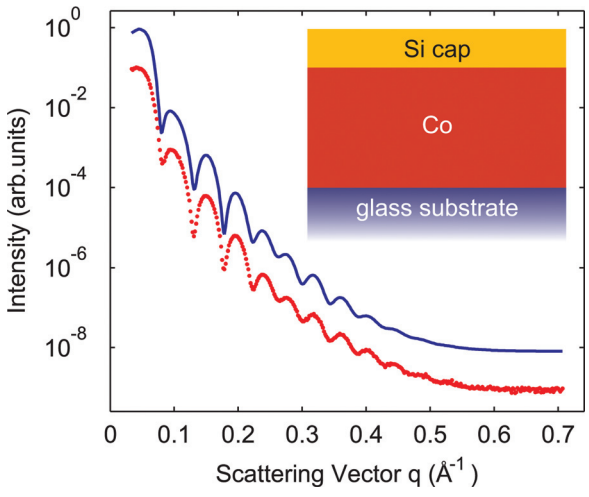

FIG. 1. (Color online) XRR measurement of an exemplary Co film (dots, lower curve) and simulation of the data (solid line, upper curve) by means of the presented model (inset). Si cap: 3.6 nm thickness and 0.9 nm roughness; Co film: 11.2 nm thickness and 1.4 nm roughness; glass substrate: 0.9 nm roughness. The curves are shifted for clarity.

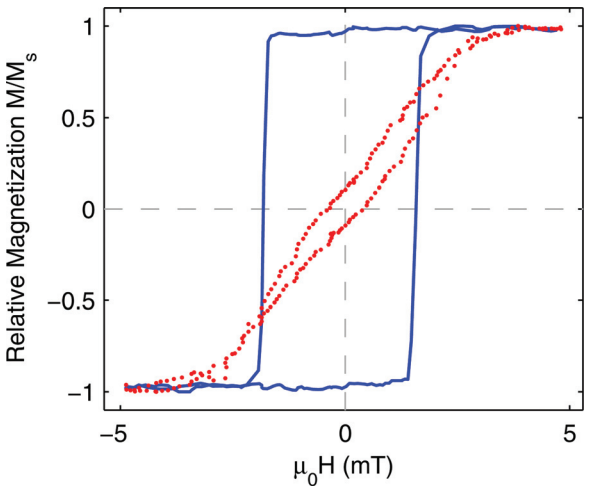

FIG. 2. (Color online) MOKE measurement of 50 nm Co on glass: magnetization curve along the magnetic easy axis at an azimuthal sample angle of $\Phi = 150°$ (solid line) and along the magnetic hard axis at $\Phi = 54°$ (dotted line) with respect to one common edge of the glass substrate.

recorded at an azimuthal sample angle of $\Phi = 150°$ with respect to the glass substrate edge. The curve represents a magnetic easy axis, i.e., square-loop behavior with considerable coercive field strength and magnetic remanence M_r nearly reaching the saturation magnetization. A second magnetization curve at $\Phi = 54°$ shown in Fig. 2 (dotted curve) exhibits the magnetic behavior of a magnetic hard axis. Here, the coercive field strength is relatively low and the magnetic remanence M_r nearly vanishes.

The presence of such a strong magnetic in-plane anisotropy with magnetic easy and hard axis is surprising because the amorphous structure of the glass substrate usually leads to an amorphous or polycrystalline growth of the Co film. So, the origin of this anisotropy cannot be a magnetocrystalline behavior of a unicrystalline structure. Whereas, for instance, this is the case for epitaxial Co films on single crystalline MgO substrates[10] or on $FeCu_3$ buffer layers on GaAs substrates,[11] respectively. Thus, another influence from the substrate is responsible for this result or a texture in a polycrystalline growth mode could effect this anisotropy as reported in Ref. 12 for polycrystalline Co films on single crystalline Si and on glass substrates.

In order to analyze the complete in-plane magnetic behavior of the 50 nm Co film, more magnetization curves are examined at different in-plane directions characterized by the azimuthal sample angle Φ. These curves show hystereses with intermediate behavior between magnetic easy and hard axis. The squareness M_r/M_s of these curves is plotted against the azimuthal sample angle Φ with respect to the edge of the glass substrate as presented in Fig. 3(a). One can see a two-fold uniaxial magnetic anisotropy with one magnetic easy axis at $\Phi = 150°$ (maximum value of the squareness) and one magnetic hard axis perpendicular to this at $\Phi = 60°$ (minimum value of the squareness).

The magnetization curves of the thickest Co film on glass (90 nm) on glass are different from the curves of the 50 nm Co film. The squareness plotted in polar coordinates rather shows a four-fold magnetic anisotropy as presented in Fig. 3(b). A second magnetic easy axis perpendicular to the first one is obtained. The directions of the magnetic easy axes are $\Phi = 0°$ and $\Phi = 90°$. This is due to the edges of the square-shaped sample because of the shape anisotropy.

An exemplary ultra-thin Co film (11.2 nm thickness) shows a UMA similar to the 50 nm Co film. Figure 4(a) presents the angular dependence of the squareness determined for this film. The direction of the magnetic easy axis amounts to $\Phi = 170°$. For another thin Co film (14.5 nm thickness) the magnetic hard axis is less pronounced as for the 11.2 and 50 nm Co film as presented in Fig. 4(b). Furthermore, the angle of the magnetic easy axis is about $\Phi = 40°$.

Summarizing the results for all ultra-thin Co films (film thickness <20 nm), we observe a UMA with more or less

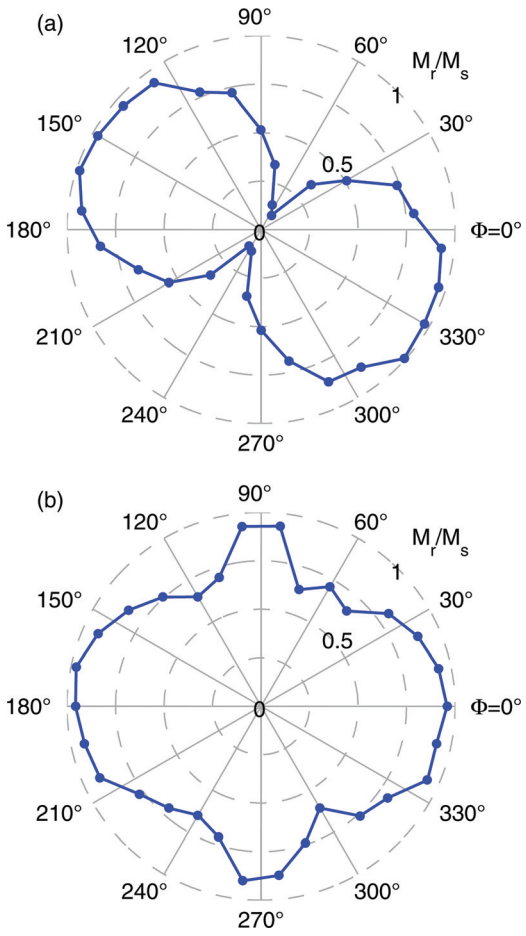

FIG. 3. (Color online) Squareness M_r/M_s plotted against the azimuthal sample angle Φ for Co films with a thickness of (a) 50 and (b) 90 nm.

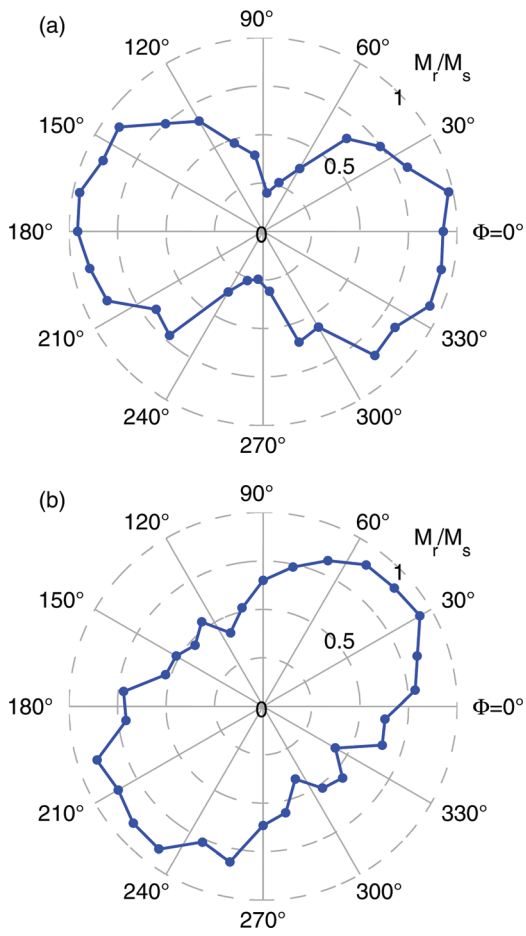

FIG. 4. (Color online) Squareness M_r/M_s plotted against the azimuthal sample angle Φ for Co films with a thickness of (a) 11.2 and (b) 14.5 nm.

pronounced magnetic easy axis. The directions of the magnetic easy axes differs from sample to sample, although the preparation conditions such as angle of incidence of the molecular beam and substrate treatment were identical.

Furthermore, substrate strain can be excluded as an origin of the UMA, because the glass substrates were cut out of the same glass plate and so preferred directions should be identical for all samples. Additionally, some substrates were carefully annealed and cooled down slowly before transferred into the vacuum chamber to eliminate possible strain of the glass substrates. Nevertheless, the UMA is still present for Co films deposited on these preannealed substrates. Strain caused by fixing the substrate onto the preparation sample holder can also be excluded, since some substrates were mounted 90° in-plane rotated with respect to other samples. Nevertheless, the direction of the UMA of the 90° rotated films did not rotate by 90°. Thus, in summary we cannot obtain any correlation between preparation conditions and direction of the UMA.

The azimuthal dependence of M_r can be modeled to determine the direction of the magnetic easy axes more precisely. Assuming that the magnetization vector is parallel to the magnetic easy axis for vanishing external field, the projection of the in-plane magnetization vector to the plane of incidence of light is a cosinelike function as demonstrated in Fig. 5(a). Because of the two-fold symmetry of the anisotropy, the fitting function

$$\frac{M_r}{M_s} = \frac{M_r^{max}}{M_s}\left|\cos(\Phi - \Phi_0)\right| + \frac{M_r^{off}}{M_s} \quad (1)$$

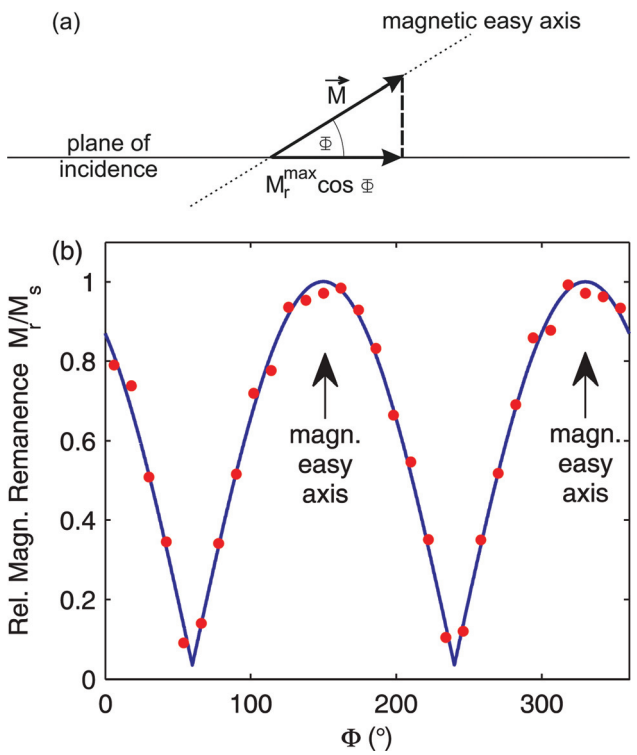

FIG. 5. (Color online) (a) Projection of the in-plane magnetization $\vec{M}$ in magnetic remanence to the plane of incidence of light. (b) Fitting function (solid line) for the relative magnetic remanence (squareness) of the 50 nm Co film plotted against the azimuthal sample angle Φ (dots) using Eq. (1) with an amplitude $M_r^{max}/M_s = 0.97$, an offset $M_r^{off}/M_s = 0.035$ and a phase $\Phi_0 = 150°$.

was chosen. The fitting parameters are the amplitude M_r^{max}/M_s (strength of the UMA), the offset M_r^{off}/M_s (isotropic contribution, background) and the phase Φ_0 (direction of magnetic easy axis). For the 50 nm Co film the relative magnetic remanence (squareness) in cartesian coordinates and the fitted curve are presented in Fig. 5(b). The phase Φ_0 gives the direction of the magnetic easy axis (maximum of magnetic remanence).

Having determined the directions of the magnetic easy axes of all ultra-thin Co films using the analysis technique just described, one can easily compare the results to the thickness of the samples. A thickness-dependent rotation effect is obtained as shown in Fig. 6(a). The angle of the magnetic easy axis decreases with increasing thickness of the Co film. Here, the angle of the magnetic easy axis is determined with respect to one common substrate edge of the bigger glass plate from which the substrates were cut out before preparation.

In order to test the influence of the shape anisotropy, the angle of the magnetic easy axis with respect to the nearest substrate edge is plotted against the Co film thickness in Fig. 6(b). For the thinnest Co films (thickness <14 nm) there

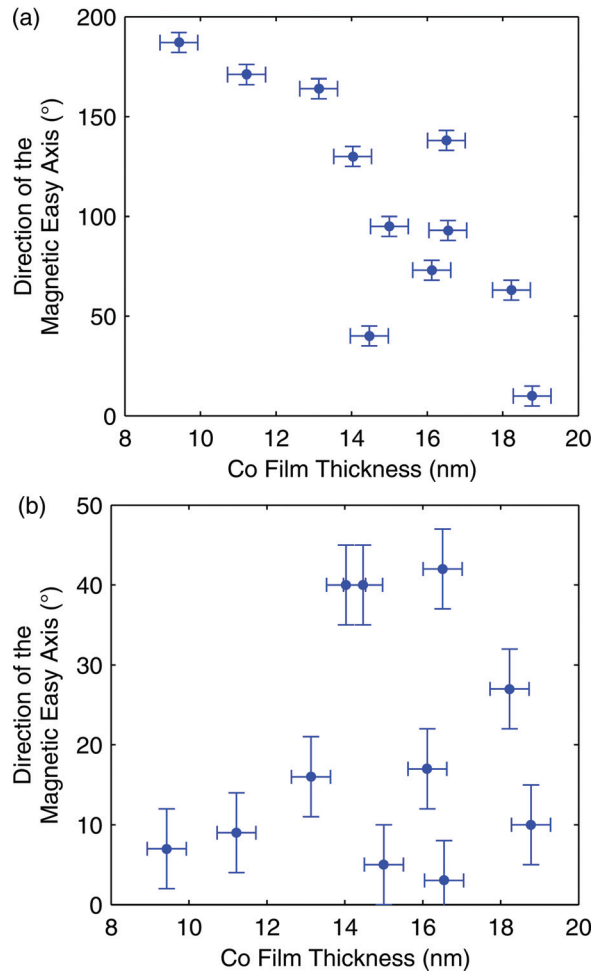

FIG. 6. (Color online) Direction of the magnetic easy axis plotted against the Co film thickness for the ultra-thin Co films. (a) Direction with respect to one common substrate edge of the bigger glass plate, of which the substrates were cut out. (b) Direction with respect to the nearest substrate edge to test the influence of the shape anisotropy.

seems to be an influence of the shape anisotropy to the direction of the magnetic easy axis. This direction is more orientated to the nearest substrate edge (direction of 0°) as it is the case for the thicker films (thickness $\geq$14 nm), which seem to be neglectably influenced by the shape anisotropy.

C. GIWAXS results

The UMA may have a magnetocrystalline origin, which may not be correlated with the investigated external parameters for film deposition. Therefore, the structure of the films is also determined by GIWAXS. So, grazing incident x-rays and wide diffraction angles are used. A schematic drawing of the diffraction geometry used is presented in Fig. 7. The intensities of diffracted x-ray waves are measured depending on the diffraction angle Θ between the wavevector of incident and diffracted light, $\vec{k}_i$ and $\vec{k}_f$, respectively, as sketched in Fig. 7(a). Areas of higher intensity in the 2D diffraction pattern are due to intersections between the Bragg sphere (due to the polycrystalline structure of the Co film) and the Ewald sphere in reciprocal space [Fig. 7(b)].

The diffraction pattern of the 14.2 nm Co film shows two broadened reflections as presented in Fig. 8(a). The upper reflection 'A' is less intense and belongs to the amorphous Co film due to short range correlations (next neighbor distance). The more intense reflection 'B' for smaller scattering angles is due to the amorphous structure of the silica glass substrate and the Si capping layer.

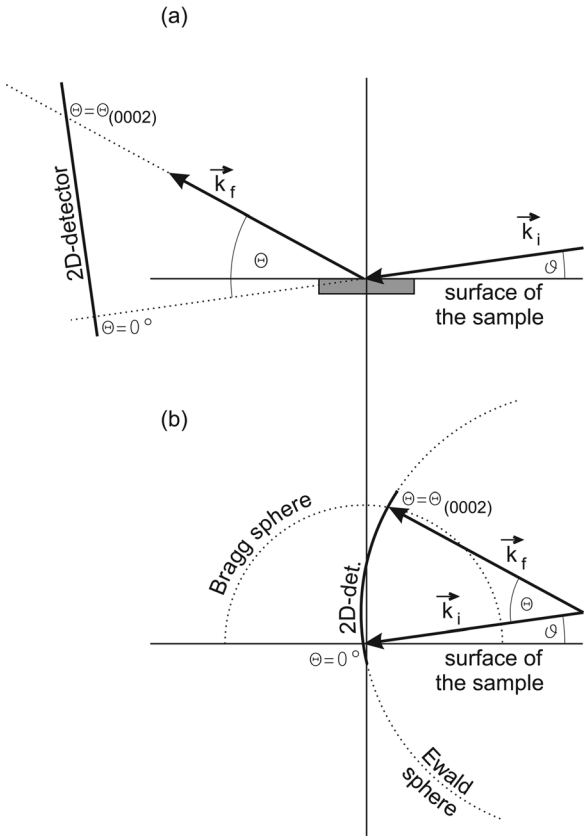

FIG. 7. Principle drawing of the GIWAXS geometry used. $\vec{k}_i$, $\vec{k}_f$: wavevector of the incident and diffracted x-ray beam, respectively, ϑ: angle of incidence of x-ray beam, Θ: scattering angle of x-ray beam. (a) real space. (b) reciprocal space.

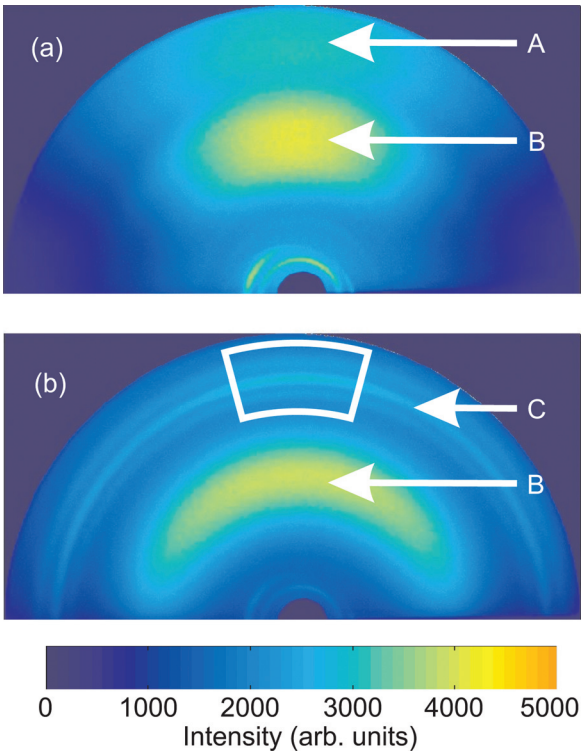

FIG. 8. (Color online) Diffraction pattern of the (a) amorphous 14.2 nm Co film and (b) polycrystalline 50 nm Co film. The upper 30° section as indicated by white lines is azimuthally integrated in Fig. 9. Both patterns are measured for an azimuthal sample angle of $\Phi = 0°$. A: Amorphous Co Bragg reflection. B: Amorphous Si Bragg reflection. C: Polycrystalline Co Bragg reflection.

In contrast to this, the 50 and 90 nm Co films clearly have polycrystalline structure as shown by the sharp rings 'C' in the diffraction pattern in Fig. 8(b). This diffraction rings are due to the $(10\bar{1}0)$-, (0002)-, and $(10\bar{1}1)$-Bragg conditions of the hexagonal structure of the Co crystallites. Although in diffraction patterns of Co powder the $(10\bar{1}1)$-ring is the strongest one,[13] in our measurement the (0002)-ring is the most intense one. This indicates that the (0001)-direction is favored for the Co crystallites we measured.

After azimuthal averaging the intensity of the upper 30° section as indicated by white lines in Fig. 8(b), the Bragg peaks can be fitted with Gaussians as presented for the 50 nm Co film in Fig. 9 to determine the lattice parameters. The positions of the Bragg peaks yield the hexagonal lattice constants $a = 2.49$ Å and $c = 4.10$ Å, which are close to the bulk values. The lattice constant a is 0.8% lower than the bulk value of $a_{bulk} = 2.51$ Å and the lattice constant c is 0.7% increased compared to the bulk constant $c_{bulk} = 4.07$ Å pointing to some tetragonal distortion of the crystal lattice.

The average crystallite size S of the $\langle 10\bar{1}0\rangle$- and $\langle 0002\rangle$-oriented Co crystallites can be calculated from the FWHM $\Delta\Theta$ and the position Θ of the Bragg peaks using the Scherrer formula

$$S = \frac{\lambda}{\cos(\frac{\Theta}{2})\Delta\Theta} \tag{2}$$

with the wavelength λ of the x-ray light. We obtain $S = 55.3$ Å for the $\langle 10\bar{1}0\rangle$-oriented and $S = 52.6$ Å for the $\langle 0002\rangle$-oriented

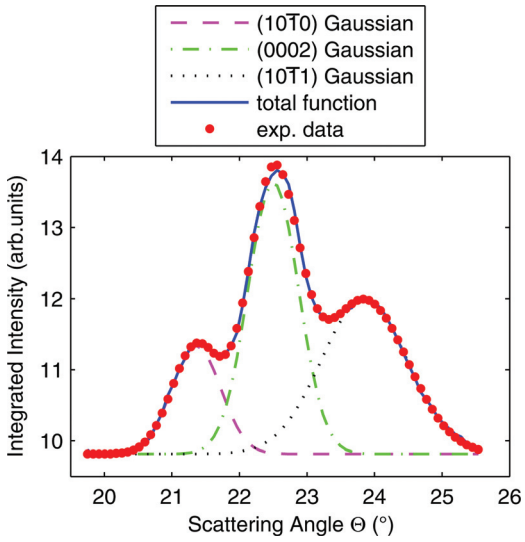

FIG. 9. (Color online) Azimuthally integrated intensity for the 50 nm Co film. The upper 30° section as indicated by white lines in Fig. 8(b) is used for integration. The intensity is plotted against the diffraction angle Θ for the azimuthal sample angle of Φ = 0°. The hexagonal Bragg peaks are fitted with Gaussians.

crystallites. So, no asymmetric crystallite shapes due to preferred growth of crystallites in distinct crystalline directions are observed.

The nonspecular diffraction geometry allows to probe the polycrystalline structure of the Co film for various lateral directions. Therefore, for the 50 nm Co film diffraction patterns are recorded for different azimuthal sample angles Φ. The polycrystalline diffraction rings for different angles Φ are analyzed with respect to the lattice parameters to study azimuthal strain effects of the Co film. The results are shown in Fig. 10. The qualitative progress of the Bragg intensities in Fig. 10(a) is comparable and has a maximum at Φ = 42°. Compared to the directions of the magnetic easy axis at Φ = 150° (continuous line) and the magnetic hard axis at Φ = 60° (dashed line) observed by MOKE, however, there is no correlation between the magnetic anisotropy and film morphology observable. For all orientations of the sample both the lateral and vertical lattice constants *a* and *c*, respectively, are close to the bulk value as shown in Fig. 10(b). Obviously, there is also no two-fold correlation to the magnetic anisotropy detectable. On the one hand, the average crystallite sizes of the ⟨10$\bar{1}$0⟩- and ⟨0002⟩-oriented crystallites (as obtained from the Scherrer formula) in Fig. 10(c) are nearly the same for small sample angles Φ. On the other hand, for large angles they differ with a minimum (S = 37.7 Å) for the ⟨10$\bar{1}$0⟩-oriented and a maximum (S = 74.7 Å) for the ⟨0002⟩-oriented crystallites at Φ = 203°. However, no correlation to the magnetic anisotropy is obtained here, too.

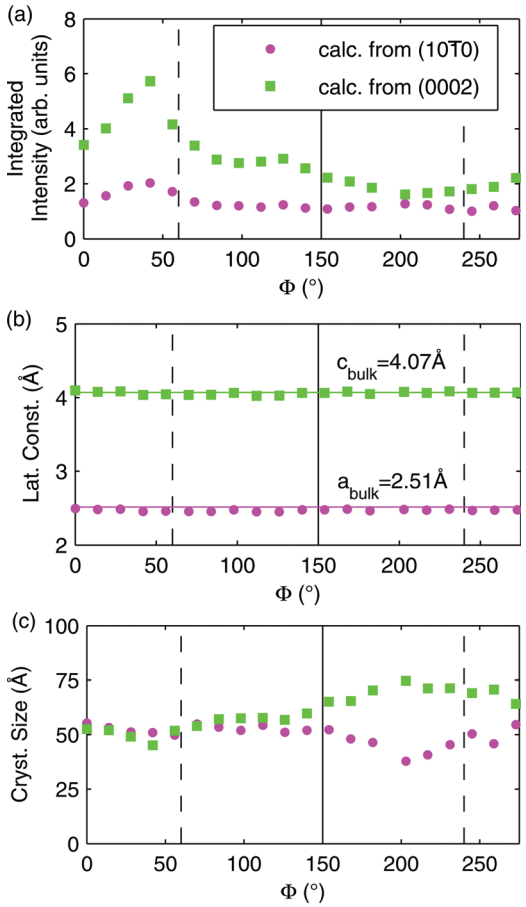

FIG. 10. (Color online) (a) The integrated intensities of the Bragg peaks for the 50 nm Co film. (b) The lattice constants *a* and *c* calculated from the diffraction angle Θ of the Bragg peak positions. (c) The average crystallite size S for the ⟨10$\bar{1}$0⟩- and ⟨0002⟩-oriented crystallites calculated from the FWHM of the Bragg peaks using Eq. (2). Circles: calculated from the (10$\bar{1}$0) peak. Squares: calculated from the (0002) peak. Continuous vertical line: magnetic easy axis. Dashed vertical line: magnetic hard axis.

IV. DISCUSSION

This work is dedicated to study the origin of the UMA for Co films deposited on glass substrates. Finally, having examined various parameters several possible reasons for this effect can be excluded. The preparation conditions like the angle of incidence of the molecular beam, temperature of the substrate during deposition or even deposition rate cannot be the reason for the UMA. All of these parameters were kept constant for the thinner Co films, but nevertheless the direction of the resulting magnetic anisotropy differs for each sample. In Ref. 1 the angle of incidence of the molecular beam amounts to 30° with respect to the surface normal, in Ref. 2 the angle is 45°. For both the obliqueness of deposition is assumed to be the reason for the observed UMA for Fe films on MgO. Here, however, we used almost normal incidence, so that no direction is preferred from the incident molecular beam.

In Ref. 5, it is assumed for Co films on glass that strain in the substrate or surface polish could be the origin of UMA. Our measurements demonstrate that theses points cannot explain the effect. Some substrates were carefully annealed and cooled down slowly before entering the vacuum chamber to reduce strain in the glass. But nevertheless, these samples show the typical magnetic anisotropy after the Co film has been grown and, furthermore, different directions of the magnetic easy axis were obtained. Also, possible strain caused by fixing the substrate in the preparation sample holder can be excluded. Substrates were built in 90° rotated around the surface normal and no correlation for the UMA compared to the

nonrotated samples was obtained. To check for effects caused by linear defects as scratches in the surface of the substrates, some glass plates were prepared with marks along one direction (approximately 3 μm wide and 0.5 μm deep). But again, these samples show no correlations between the direction of the magnetic anisotropy and the direction of induced microstructure defects (for details see Ref. 14).

The substrate shape could induce a magnetic shape anisotropy, if the samples had a two-fold geometry. But all our samples have square shape, so if there were any magnetic shape anisotropy additional to the in-plane preference, it had to be four-fold and it should correlate identically on the glass substrate shape for all samples. This, however, is not the case for most of the samples. Only the thickest Co film (90 nm thickness) shows a two-fold magnetic anisotropy with two magnetic easy axes, which can be interpreted as a four-fold magnetic anisotropy combined with a UMA. It also could be interpreted as a more isotropic magnetic behavior because of the thicker and therefore more homogeneous Co film. For all other samples we observe only one easy axis. However, if one of the two magnetic easy axes induced by the square shape anisotropy is more pronounced due to additional effects the main magnetic easy axis should be orientated to one substrate edge. In our experiments this is only the case for very thin films (film thickness <14 nm) or for the thickest one (film thickness 90 nm). Thus, the magnetization of the samples may be governed by the shape anisotropy.

The thickness of the films affects the atomic structure. Thinner films are amorphous, whereas the thicker ones show a polycrystalline structure. It is shown in Ref. 12 that there is a transition from amorphous to polycrystalline structure below the Co film thickness of 173 nm. Furthermore, RHEED patterns in Ref. 15 have shown that the growth of 25 nm Co films on glass is quite disordered. The films, however, have microcrystalline structure. In Ref. 6, crystallites with a size below 5 nm are still detected for a 20 nm Co film. These results are comparable to our measurements.

The difference of the preparation conditions between the ultra-thin Co samples (film thickness <20 nm) and the thicker samples (film thickness ≥ 50 nm) could be responsible for the different growth modes, too. For example, the deposition rate was higher and the pressure in the chamber lower for the thick samples than for the thin ones. Nevertheless, all samples show a magnetic two-fold anisotropy, so the growth mode cannot be an explanation for the effect. Also, it can be excluded that the atomic structure of the Co film causes this UMA because we achieve UMAs in polycrystalline as well as in amorphous Co films. Even an in-plane strain effect cannot be found as a reason for this effect.

The direction of the UMA rotates depending on the Co film thickness. The angle between the magnetic easy axis and the common sample edge decreases with increasing Co film thickness. This effect cannot be explained only by the shape anisotropy. While for the thinnest Co films (film thickness <14 nm) the magnetic easy axis is orientated to the nearest sample edge, another effect should be the reason that for thicker films the magnetic easy direction is not orientated to the shape of the sample. An explanation could be that the magnetization in a homogeneous, amorphous, ultra-thin film is more sensitive to the shape anisotropy than in thicker films, which are not so homogeneously grown due to small polycrystalline parts. For a homogeneous, polycrystalline film the influence of the shape anisotropy is large again as it is the case for the 90 nm Co film. The films with intermediate thicknesses have neither homogeneously amorphous nor homogeneously polycrystalline structure. So, the influence of the structure to the anisotropy is larger than the influence of the shape. Thus, the direction of the UMA is not related to the edges of the substrate for these films. In this region of thickness the orientation of the UMA is partially not reproducible. On the one hand for the samples with 14 ± 0.5 nm Co film thickness the direction of the magnetic easy axis related to the nearest substrate edge is identical. On the other hand for the samples with 16 ± 0.5 nm Co film thickness the orientations of the magnetic easy axes differ from sample to sample [cf. Fig. 6(b)].

Another explanation for a UMA could be an external magnetic field, which influences the preparation procedure. If this would be the case, the magnetic field has to change from sample preparation to sample preparation, because the direction of the magnetic easy axis changes. In addition, we did not observe any systematic variation of UMA which correlates to the sequence of sample preparation.

V. CONCLUSION

Co films of different thicknesses (between 8.5 and 90 nm) were grown by MBE. The films were examined regarding their magnetic anisotropy by means of the MOKE. The structural characterization was mainly performed by XRR and GIWAXS. Furthermore, AFM was used.

All films reveal a magnetic easy and hard axis and therefore a UMA except the thickest one of 90 nm thickness, which shows two easy axes perpendicular to each other. For the origin of the UMA influences like preparation conditions, textures in the film structure, strain in the substrate and obliqueness of deposition can be excluded from our measurements. The direction of the UMA depends on the thickness of the Co film. With increasing Co film thickness the angle of the easy axis decreases with respect to the orientation of the substrate edge. The shape anisotropy cannot be the only reason for this effect because the magnetic easy direction for only the thinnest films (film thickness <14 nm) and the thickest one (film thickness 90 nm) is orientated to the nearest sample edge. The homogeneity of the structure could generate a larger influence of the shape anisotropy to the direction of the magnetic easy axis. For the thinnest, homogeneously amorphous and for the thickest, homogeneously polycrystalline grown films the influence of the shape anisotropy is stronger and thus, the UMA is orientated to the substrate edge. For the films with intermediate thickness the direction of the UMA is not related to the substrate edge because of the stronger magnetocrystalline influence of the more inhomogeneous structure.

ACKNOWLEDGMENTS

We thank Christian Sternemann for his support at beamline BL9 at DELTA. Portions of this research were carried

out at the light source DORIS III at DESY. DESY is a member of the Helmholtz Association (HGF). We would like to thank Wolfgang Caliebe for assistance in using beamline W1. We also thank Jaroslav Hamrle from the Technical University of Ostrava (Czech Republic) for the intense discussion on MOKE measurements and techniques.

We acknowledge financial support by Deutsche Forschungsgemeinschaft (DFG) via Graduate College 695 and Ph.D. program of Lower Saxony, Germany.

[1]O. Durand, J. R. Childress, P. Galtier, R. Bisaro, and A. Schuhl, J. Magn. Magn. Mater. **145**, 111 (1995).
[2]Y. Park, E. E. Fullerton, and S. D. Bader, Appl. Phys. Lett. **66**, 2140 (1995).
[3]Y. Z. Wu, C. Won, and Z. Q. Qiu, Phys. Rev. B **65**, 184419 (2002).
[4]W. Yang, D. N. Lambeth, and D. E. Laughlin, J. Appl. Phys. **87**, 6884 (2000).
[5]J. B. Wedding, M. Li, and G.-C. Wang, J. Magn. Magn. Mater. **204**, 79 (1999).
[6]B. Presa, R. Matarranz, M. C. Contreras, J. F. Calleja, L. E. Fernandez-Outon, and K. O'Grady, IEEE Trans. Magn. **44**, 2788 (2008).
[7]L. G. Parratt, Phys. Rev. **95**, 359 (1954).
[8]F. Bertram, Bachelor thesis, University of Osnabrück (2007).
[9]R. M. Osgood III, S. D. Bader, B. M. Clemens, R. L. White, and H. Matsuyama, J. Magn. Magn. Mater. **182**, 297 (1998).
[10]Y. Nukaga, M. Ohtake, M. Futamoto, F. Kirino, N. Fujita, and N. Inaba, IEEE Trans. Magn. **45**, 2519 (2009).
[11]X. Xu, L. Yin, G. Dong, and X. Jin, Phys. Rev. B **80**, 092405 (2009).
[12]A. Kharmouche, S.-M. Chérif, A. Bourzami, A. Layadi, and G. Schmerber, J. Appl. Phys. D: Apl. Phys. **37**, 2583 (2004).
[13]L. J. E. Hofer and W. C. Peebles, J. Am. Chem. Soc. **69**, 893 (1947).
[14]T. Becker, Dipoma thesis, University of Osnabrück (2008).
[15]C. Marliére, D. Renard, and J. P. Chauvineau, Thin Solid Films **201**, 317 (1991).